Rethinking of Black-Carbon Associated Organic Particles: Insights into Aged Biomass Burning Organic Aerosol

Junfeng Wang[†,‡,*], Jianhuai Ye[‡], Dantong Liu[⸸], Yangzhou Wu[⸸], Jian Zhao[§], Weiqi Xu[§], Conghui Xie[§], Fuzhen Shen[†], Jie Zhang[⊥], Paul E. Ohno[‡], Yiming Qin[‡], Xiuyong Zhao[¶], Scot T. Martin[‡], Alex K.Y. Lee[⁋], Pingqing Fu[†], Daniel J. Jacob[‡], Qi Zhang[†], Yele Sun[§], Mindong Chen[†] and Xinlei Ge[†,*]

[†]Jiangsu Key Laboratory of Atmospheric Environment Monitoring and Pollution Control, School of Environmental Science and Engineering, Nanjing University of Information Science and Technology, Nanjing, China
[‡]School of Engineering and Applied Sciences, Harvard University, Cambridge, MA, United States
[⸸]Department of Atmospheric Sciences, School of Earth Sciences, Zhejiang University, Hangzhou, China
[§]State Key Laboratory of Atmospheric Boundary Layer Physics and Atmospheric Chemistry, Institute of Atmospheric Physics, Chinese Academy of Sciences, Beijing, China
[⊥]Department of Atmospheric Science, Colorado State University, Fort Collins, CO, United States
[¶]State Environmental Protection Key Laboratory of Atmospheric Physical Modeling and Pollution Control, State Power Environmental Protection Research Institute, Nanjing, China
[⁋]Department of Civil and Environmental Engineering, National University of Singapore, Singapore
[†]Institute of Surface-Earth System Science, Tianjin University, Tianjin, China
[†]Department of Environmental Toxicology, University of California Davis, Davis, CA, United States

*Corresponding author: Xinlei Ge (Email: caxinra@163.com); Junfeng Wang (wangjunfeng@g.harvard.edu).

Submitted to ***Environmental Science & Technology***

ABSTRACT

Black carbon (BC) particles in Beijing summer haze play an important role in regional radiation balance and related environmental processes. Understanding the factors that lead to variability in the impacts of BC remains limited. Here, we present observations by a soot-particle aerosol mass spectrometer of BC-containing submicron particulate matter (BC-PM_1) in the summer of 2017 in Beijing, China. These observations were compared to concurrently measured total non-refractory submicron particulate matter (NR-PM_1) by a high-resolution aerosol mass spectrometer (HR-AMS). Distinct variations were observed between NR-PM_1 and BC-PM_1 related to organic aerosol (OA) composition with hydrocarbon-like OA in BC-PM_1 up to two-fold higher than that in NR-PM_1 in fresh vehicle emissions, suggesting that a part of HOA in BC-PM_1 may be undetectable by HR-AMS. Cooking-related OA was only identified in NR-PM_1, whereas aged biomass burning OA (A-BBOA) was a unique factor only identified in BC-PM_1. The A-BBOA was linked to those heavily coated BC, which may lead to enhancement of light absorption ability of BC by a factor of two via the "lensing effect". More-oxidized oxygenated OA identified in BC-containing particles was found to be slightly different from that observed by HR-AMS, mainly due to the influence of A-BBOA. Overall, these findings highlight that BC in urban Beijing in June is partly of agricultural fire origin and, an unique biomass burning-related OA associated with BC may be ubiquitous in aged BC-PM_1, and this OA may play a role in regional energy balance that has not previously been fully considered.

1. INTRODUCTION

Black carbon (BC) is an important component of atmospheric aerosol that exerts negative effects on regional radiation balance[1] and human health.[2] It absorbs solar radiation, leading to direct atmospheric heating.[3] Indirectly, BC particles can also serve as cloud condensation nuclei upon mixing with hydrophilic species (e.g., sulfate), resulting in changes in cloud properties.[4] Inhalation of BC is associated with adverse health impacts such as respiratory and cardiovascular diseases, cancers, and birth defects.[2]

Black carbon particles are released to the atmosphere directly from incomplete fuel combustion and open fires.[1, 3] Non-BC species (e.g., inorganic and organic) can coat onto BC particles in the atmosphere through condensation and/or coagulation processes[5]. These atmospheric processes (also known as "aging") gradually alter the mixing state and the morphology (e.g., from an externally-mixed fractal structure[6] into an internally-mixed "core-shell" structure[7]) of submicron BC-containing particles, (BC-PM_1). These alterations can enhance the light absorption capacity of the BC core via the "lensing effect" due to the increased light absorption cross-section as a result of the enhanced coating thickness[8, 9]. Additionally, the chemical constituents of BC-PM_1 may dynamically change during the aging processes, also lead to changes in the light absorption capacity of the particles. Because these physical and chemical processes of both organic and inorganic species inside BC-PM_1 continuously alter particle properties throughout the lifetime of the particles, great uncertainty remains in quantifying the light absorption ability of BC. Understanding the relationship of BC mixing state and chemical composition to the light absorption properties of BC-PM_1, as well as its spatiotemporal distribution, is of importance to accurately evaluate the impacts of BC in regional air quality.

Aerodyne high-resolution aerosol mass spectrometry (HR-AMS)[10] has been widely applied in field studies to investigate the chemically-resolved composition of non-refractory submicron particulate matter (NR-PM_1, species that vaporize at temperature < 600 °C)[11-17]. However, the working temperature of the standard HR-AMS tungsten vaporizer (600 ºC) is not sufficient to vaporize refractory species such as BC. To overcome this limitation, soot-particle aerosol mass spectrometry (SP-AMS) is developed[18]. In addition to the standard tungsten vaporizer, SP-AMS is equipped with a laser vaporizer (with a wavelength of 1064 nm) which selectively heats BC, together with the non-BC species mixed with it.[19] This novel technique makes it possible to

compare the compositions of BC-PM_1 and NR-PM_1, allowing a more accurate assessment of the impacts of BC.

There have only been a few studies that have compared the differences of species analyzed by BC-PM_1 and NR-PM_1.[5, 20, 21] Lee et al.[5] found that cooking-related organic aerosol (COA) may externally mix with BC in summertime California. The COA factor was identified in NR-PM_1 organic aerosol (OA), but not the BC-related OA. Wang et al.[22] found that transported biomass burning organic aerosol could be thickly coated on BC in central Tibetan Plateau and significantly enhance the light absorption capacity of BC cores. Interestingly, the transported biomass burning organic aerosol was not resolved in NR-PM_1 OA particles from concurrent HR-AMS measurements[23]. These studies suggest that BC-related OA may undergo different atmospheric processes compared to those do not contain BC.

Beijing is a megacity known for high particulate matter (PM) concentrations. BC-PM_1 during haze events of summertime Beijing may have distinct sources and properties than other locations in the world. In this study, we focus on the differences of individual species between BC-PM_1 and NR-PM_1 regarding their chemical composition, mass loadings, sources, and formation pathways in summertime in urban Beijing. Results from this study provide a better understanding of the formation mechanism of OA particles in Beijing haze and valuable insights in assessing their impacts on air quality.

2. EXPERIMENTAL METHODS

2.1. Sampling site and period

The observations were conducted at a rooftop laboratory (8 m above ground level) in the Tower Division of the Institute of Atmospheric Physics (IAP), Chinese Academy of Sciences (CAS) in urban Beijing (39° 58′ N, 116° 22′ E), China, from 4 to 29 June, 2017. This site has been reported multiple times to be a typical urban observation location[24-29]. The site is located around the North 3rd Ring Road of Beijing. A highway is approximately 360 m to the east and a lot of restaurants (e.g., Sichuan style and BBQ) are within 100 m on the north side.

2.2. Instrumentation

Two Aerodyne Aerosol Mass Spectrometers (AMS), including a laser-only Soot-Particle AMS (SP-AMS) and a standard High-Resolution Time of Flight AMS (HR-AMS) were deployed to collect chemical composition and size distributions of BC-PM_1 and NR-PM_1, respectively. Three types of species were measured during the campaign: BC-free NR-PM_1 species (Type I), NR-PM_1 species mixed with BC and can be detected by HR-AMS (Type II), and total BC-containing PM_1 including BC cores and all coated species (Type III). HR-AMS is capable of measuring Type I and Type II, while laser-only SP-AMS can measure Type II and Type III. A shared $PM_{2.5}$ cyclone inlet (Model URG-2000-30ED) with 3 Lpm flowrate and a diffusion dryer were used prior to the sampling. The detailed information on the operation of HR-AMS and SP-AMS during the sampling campaign can be found in previous literature[29, 30]. Details of tuning, calibration, and configurations of the two AMS instruments can be seen in our previous papers[26, 28, 30]. Mixing ratios of O_3, and NO_2 (Thermo Fisher Scientific, model 49*i* and model 42C) were measured in parallel simultaneously. Vertical meteorological parameters, including temperature (*T*) and relative humidity (*RH*), were measured from the IAP 325m meteorological tower.

2.3. Data Analysis

AMS data analysis was performed by using Squirrel 1.57 and Pika 1.16I based on Igor Pro 6.37 (WaveMetrix Corp.). The measurement of filtered air was performed for 24 hours before the start of the campaign to determine the detection limits of various aerosol species and to adjust the fragmentation table. The relative ionization efficiency

(RIE) of BC was calibrated with Regal Black (RB, REGAL 400R pigment black, Cabot Corp.). The average ratio of C_1^+ to C_3^+ ionized from pure BC (RB) was determined to be 0.53, which minimizes the influence of C_1^+ from non-refractory organics. The RIE of BC was determined to be 0.17 based on calibrations performed before, in the middle, and at the end of the campaign. RIEs of NO_3^-, SO_4^{2-}, NH_4^+ were determined to be 1.1, 0.82, and 3.82, respectively, and default values of 1.3 and 1.4 for RIEs of Chl and Org were applied, respectively.[10] Since direct calibration of NO_3^-, SO_4^{2-}, NH_4^+ are impossible under the laser only configuration, hence, the RIEs calibration of NO_3^-, SO_4^{2-}, NH_4^+ were all obtained before the tungsten vaporizer was removed by assuming those RIEs were remain unchanged throughout the campaign.[22] Polystyrene latex (PSL) spheres (100-700 nm) (Duke Scientific Corp., Palo Alto, CA) were used to calibrate the particle size distribution before the campaign. The default collection efficiency (CE) of 0.5 were applied for both HR-AMS and SP-AMS in this study. It should be noticed that, the BC quantification will not be affected by particle bouncing without the tungsten vaporizer, which could affect the CE in the standard HR-AMS measurements.[10] However, the CE will be governed by the overlap of particle beam and laser beam.[5, 21] Both HR-AMS and SP-AMS chemically resolved mass concentrations of NR-PM_1 and BC were calculated based on V-mode high-resolution fitting. Due to different vaporization schemes between the HR-AMS and SP-AMS, mass spectra from these two instruments even for the same population of aerosols are not entirely the same. Because laser-only SP-AMS generally results in less overall fragmentation, its mass profile may contain more large *m/z* fragments and less small *m/z* fragments compared to that from HR-AMS[21]. In addition, the elemental ratios of organics reported here, i.e., oxygen-to-carbon and hydrogen-to-carbon ratios (O/C and H/C) were only calculated based the "Improved-Ambient (I-A)" method[31].

Positive matrix factorization (PMF)[32] was performed on the high-resolution organic mass spectra matrix of both NR-PM_1 and BC-PM_1 (e.g., BC (C_x^+), NR-PM_1 associated with BC) across m/z 12–120 using Evaluation Tool written in Igor[33], following the standard procedure[34]. Four types of organic aerosol (OA) from total NR-PM_1 (see our previous paper)[16] and five OA factors associated with BC were identified. C_x^+ was involved in the calculation of elemental ratios (e.g, O/C and H/C) of PMF OA factors. All data presented in this paper were averaged hourly and are presented at local time (Beijing Time, UTC+8).

3. RESULTS AND DISCUSSION

3.1. Overview of observations

Figure 1 shows the temporal variations of selected chemical species during the campaign. Information for other variables is provided in the supplementary materials (SM). The two cases labeled in Figure 1 are of particular interest. Case I (June 8-13) was characterized with high NO_2 concentrations (average 26.7 ± 13.5 ppb, Table S1) and relatively low O_3 concentrations (41.7 ± 30.0 ppb) with NO_2-to-O_3 ratio of 0.64. Case II (June 17-22) was featured by low NO_2 (14.9 ± 5.9 ppb) and high O_3 (84.6 ± 30.6 ppb) concentrations with an NO_2-to-O_3 ratio of 0.18. Unlike winter Beijing haze pollution, *RH* remained at a relatively low level (36.5 ± 15.3%), which is not expected to play a significant role in OA formation during the campaign (Figure 1b and Figure S1). In contrast, a strong correlation has been observed between temperature and O_3 (r^2 = 0.53). The temperature was higher on average in Case II (29.8 ± 3.8 ºC) than in Case I (26.1 ± 4.1 ºC).

The mass concentrations and mass concentration ratios of organic (Org), sulfate (SO_4^{2-}) and nitrate (NO_3^-) in NR-PM_1 (in solid line) and BC-PM_1 (in dotted line) are shown in Figures 1c-e. High correlations were observed between BC-PM_1 and NR-PM_1 measurements for SO_4^{2-} (r^2 = 0.70) and NO_3^- (r^2 = 0.86), but not for Org (r^2 = 0.49). This result suggests that, BC-PM_1 Org has distinct sources or formation pathways from NR-PM_1 Org. Comparing two cases, the average mass ratios of BC-PM_1 to NR-PM_1 for SO_4^{2-} and NO_3^- in Case I (0.24 ± 0.11 and 0.37 ± 0.12) were close to those in Case II (0.19 ± 0.06 and 0.31 ± 0.07). However, ratios of BC-PM_1 to NR-PM_1 for Org were 160% greater for Case I (0.74 ± 0.32) compare to Case II (0.46 ± 0.13). During the nighttime, this ratio increases to almost unity in Case I. Additionally, BC concentration in Case I (average 2.6 ± 1.6 μg m^{-3}) was 1.5 folds higher than in Case II (average 1.7 ± 0.8μg m^{-3}). The implication is that the organic is mostly associated with BC and likely comprised of freshly emitted compounds in Case I. This is also evident by the moderate correlation between NO_2 and BC-PM_1 Org (r^2 = 0.42) in Case I. On the other hand, the lower Org ratio in Case II with higher O_3 concentrations indicates greater oxidation and secondary processes in non-BC particles.

3.2. Source apportionment of BC-PM_1 OA

To further investigate the differences between organics in NR-PM_1 and BC-PM_1, the comparison of PMF OA factors between NR-PM_1 and BC-PM_1 Org is necessary. Four factors were identified from PMF analysis of the NR-PM_1 Org matrix, including hydrocarbon-related OA (HOA), cooking OA (COA), less-oxidized oxygenated OA (LO-OOA), and more-oxidized oxygenated OA (MO-OOA). Details of the NR-PM_1 PMF analysis can be found in our previous paper[30]. Here we only present the PMF results of the SP-AMS measured BC-PM_1 Org. As shown in Figure 2, five OA factors were resolved by PMF with factors including a HOA, a less oxidized OOA (OOA1 or LO-OOA), three more-oxidized OOA (MO-OOA). The MO-OOA factor includes an aged BBOA (A-BBOA), a sulfate- and photochemical-related OOA (OOA2), and a nitrate-related OOA (OOA3). A key diagnostic plot of this PMF solution is presented in Figure S2.

BC-PM_1 HOA consists of a series of hydrocarbon fragments ($C_xH_y^+$) in its mass spectrum (Figure 2f), thus having a low O/C ratio (0.13) but high H/C ratio (1.62). It has a r^2 of 0.92 with $C_4H_9^+$ (m/z = 57) and a r^2 of 0.57 with NO_x (Figure 2a), indicative of its sources from vehicle emissions[35]. It also correlated tightly with BC (r^2 of 0.70) and a series of polycyclic aromatic hydrocarbons (PAHs) ions, e.g., $C_9H_7^+$ (m/z 115, r^2 of 0.63).

The second factor has a remarkably high fraction of the BBOA marker ions of $C_2H_4O_2^+$ (m/z = 60) (1.31%) and $C_3H_5O_2^+$ (m/z = 73) (1.34%) in its mass spectrum (Figure 2g), much higher than that observed in non-BBOA (e.g., 0.3% at m/z = 60) in previous studies[22, 35, 36]. As expected, the temporal variation of this factor correlated tightly with those of $C_2H_4O_2^+$ and $C_3H_5O_2^+$ (r^2 of 0.71 and 0.72, respectively). In addition, the mass spectrum of this factor is strikingly similar to that of the transported BBOA which was observed at a remote site in the central Tibetan Plateau[22], with a r^2 of 0.97. Here we categorized the transported BBOA as A-BBOA identified in this study. Similar to the A-BBOA observed in Tibetan Plateau, which has an O/C ratio of 0.51, this factor also has a relatively high O/C ratio of 0.48, greater than that of primary BBOA (O/C of 0.18−0.26)[22]. These findings support that the second factor may be associated with the oxidation of biomass burning emissions. The temporal variation of ABBOA in the Tibetan Plateau was reported to be highly correlated with the potassium ion fraction (K^+, r^2 of 0.78), and $K_3SO_4^+$ (r^2 of 0.92). However, the temporal variation of the second factor in this study is only correlated well with that of $K_3SO_4^+$ (r^2 of 0.64)

but not K^+ (r^2 of 0.01). The reason for this phenomenon is that the major source of K^+ in remote sites like the Tibetan Plateau was long-distance transport of K_2SO_4 particles, which probably from biomass burning-related K-containing salts interacts with H_2SO_4. In contrast, there are multiple primary sources of K^+ in PM_1 (e.g., diesel-vehicle emissions, and mainly KCl particles) in urban areas (Figure S3). Based on these observations, $K_3SO_4^+$ could be defined as a A-BBOA marker ion. Hence, this second factor is identified as A-BBOA that was subjected to oxidation during transport to the measurement area as presented in the bivariate polar plot and three-day back trajectories (Figure S4). June should be the month of maximum agricultural-related biomass burning in the North China Plain, although we thought that this burning had been banned in recent years because of air quality concerns.[37] The implication is that the effectiveness of banning straw burning may be overestimated.

The OOA1 factor has an O/C of 0.28 (Figure 2h). Similar to the NR-PM_1 LO-OOA[16], it is highly correlated with $C_2H_3O^+$ (r^2 of 0.72). The $C_2H_3O^+$ ion (m/z = 43) is an important component of secondary organic aerosol (SOA)[20, 38] and the diurnal patterns of the OOA1 and $C_2H_3O^+$ both show a great enhancement around noontime (Figure S5), indicating the importance of secondary formation of less oxidized organic aerosol through daytime photochemical activity.

The OOA2 factor has an O/C of 0.42 (Figure 2i) and the OOA3 factor has a smaller O/C of 0.32 (Figure 2j). OOA2 correlated strongly with sulfate (r^2 of 0.92; Figure 2d) and OOA3 correlated highly with nitrate (r^2 of 0.97; Figure 2e). These features agree well with the previously observation for low-volatility OOA (sulfate-related OOA) and semi-volatile OOA (nitrate-related OOA) in Tibetan Plateau[22].

3.3. Comparison of NR-PM_1 and BC-PM_1 OA factors

The sum of the above-mentioned BC-PM_1 A-BBOA, OOA2, and OOA3 fractions is comparable to the NR-PM_1 MO-OOA factor, based on their high O/C ratios. Figures 3a-c are comparisons of the mass loadings of HOA, LO-OOA, and MO-OOA in both NR-PM_1 and BC-PM_1. NR-PM_1 HOA, LO-OOA, and MO-OOA are strongly correlated with their counterpart fractions of BC-PM_1, with r^2 values of 0.68, 0.60, and 0.61, respectively. In Case I, most of the time, the mass loadings of BC-PM_1 HOA and MO-OOA are higher than those in NR-PM_1, while LO-OOA shows the opposite trend. In Case II, the mass loadings of BC-PM_1 HOA are also generally higher than those of NR-PM_1 HOA, however, NR-PM_1 MO-OOA and LO-OOA are almost two folds higher than those of BC-PM_1. Figures 3d-f are comparisons of the fractions of HOA, LO-OOA, and MO-OOA in NR-PM_1 and non-BC material in BC-PM_1 (coatings), respectively. In Case I, the fractions of HOA and MO-OOA internally-mixed with BC are almost two times and four times higher, respectively, than those in NR-PM_1, whereas the two LO-OOA fractions closely track each other. In Case II, two LO-OOA fractions are still overlapped, but compared to Case I, the fraction of HOA in BC-PM_1 coatings is over four times that of NR-PM_1 HOA, and the difference between the two MO-OOA fractions is smaller.

As shown in Figure 4, the average of BC-PM_1 HOA fractions (0.27 ± 0.17 and 0.11 ± 0.07, respectively) are higher than those in NR-PM_1 (0.12 ± 0.08 and 0.02 ± 0.02, respectively) in both Case I and Case II, indicating that HOA particles is more internally mixed with BC compared to other OA materials. There is a higher fraction of low-volatility HOA in BC-PM_1 that can only be evaporated under higher temperature conditions (> 600 °C) in SP-AMS. It is also possible that some species (e.g., PAHs) could be buried inside of the BC coatings or trapped in nano-carbon spheres[39], which are not readily evaporated by the tungsten vaporizer in HR-AMS. However, the possibility that RIE of OA coating may be lower than the default RIE value should also be considered. Nevertheless, previously reported HOA levels by HR-AMS need to be reinvestigated due to the possible underestimation of the refractory of HOA.

The average mass loadings of NR-PM_1 LO-OOA in both Case I and Case II were higher than those of BC-PM_1. However, the fraction of LO-OOA in both NR-PM_1 and BC-PM_1 coatings were very close to each other during the two cases, with an average value of 0.23 ± 0.10 and 0.25 ± 0.12, respectively, indicating that the probability of LO-OOA condensation onto the two different types of particles is similar.

A greater difference between the MO-OOA fractions in NR-PM_1 and BC-PM_1 was

observed in Case I than in Case II, and there is more MO-OOA in BC-PM_1 than in NR-PM_1 in Case I. A similar comparison between NR-PM_1 MO-OOA with BC-PM_1 MO-OOA without A-BBOA can be found in SI (Figure S6), which shows closer fractions in both Case I and Case II. Therefore, one possibility which may cause higher MO-OOA fraction in BC-PM_1 than that in NR-PM_1 in Case I is the presence of the BC-PM_1 A-BBOA, which is only identified from the BC-PM_1 OA. More details of the BC-PM_1 A-BBOA are discussed in Section 3.4.

3.4. Characteristics of A-BBOA in BC-containing PM_1

Figure 5 shows the high-resolution mass spectra of A-BBOA observed in Nam Co (June 2015) and Beijing (June 2017) by laser-only SP-AMS. A mass spectra very similar to that observed in Beijing was also observed in Nanjing (February 2017)[4], with a r^2 of 0.95. The A-BBOA observed in Nam Co (the Tibetan Plateau) was found in the thickest coated and internally-mixed BC-PM_1 (the mass ratio of coatings to BC core (R_{BC}) can reach 14), which enhances the light absorption ability (E_{abs}) of the BC core by a factor of 1.5 to 2.0 via the "lensing effect".

As shown in Figure 6, A-BBOA was associated with those large particles (D_{va} > 300nm) which were also heavily-coated (R_{BC} > 9, Figure 6a and 6c). Because A-BBOA is a moderately aged OA, the OSc was very steady when R_{BC} > 9 (Figure 6c). Figure 6b presents the fractions of the OA factors (left) and the degree of light absorption enhancement (E_{abs}, estimated by the mass ratios of BC measured by aethalometer model 33 and SP-AMS), as a function of R_{BC}. Figure 6d shows the temporal variations of the fractions of NR-PM_1 OA and BC-PM_1 OA from 15:00 to 24:00 on June 17, 2017 when the highest A-BBOA concentrations were observed. There is a significant enhancement of A-BBOA which may account for up to 60% of the total OA coatings, which could enhance the BC-PM_1 MO-OOA fraction (within the purple frame in the bottom panel of Figure 6d).

In this study, A-BBOA was only observed by SP-AMS and was indeed only associated with BC. It is likely that A-BBOA was emitted together with BC when burning biomass fuel, and was oxidized subsequently during the transport. However, we cannot exclude the possibility that A-BBOA can be detected by HR-AMS. For example, it might be included in NR-PM_1 MO-OOA factor. Without separating A-BBOA from other organic species, the source apportionment for HR-AMS may obscure air-quality- and climate-related implications of A-BBOA in the atmosphere, such as the enhancement of aerosol light absorption ability (Figure 6b).

4. ATMOSPHERIC IMPLICATIONS

Online chemical characteristics of BC and its associated species was for the first time elucidated in urban Beijing in summer, and compared with those of NR-PM_1 species. The biggest difference between the two measurements was in the composition of the organic species. In particular, we found BC in urban Beijing in June is partly of agricultural fire origin and, an unique biomass burning-related OA factor (A-BBOA) which was moderated aged, only existed in thickly coated BC-PM_1 (R_{BC} > 9), but not NR-PM_1. The unique A-BBOA could make up a significant portion of BC coating material. In addition to Beijing, the A-BBOA was also identified in other locations (such as central Tibet Plateau[22] and Nanjing[4]), suggesting that it may be ubiquitously presence in BC-PM_1 in the atmosphere.

BBOA species are known to constitute a large portion of light-absorbing organics (brown carbon, BrC). The delay of BBOA oxidation and its longer duration time on BC cores can extend the impacts of BC. Moreover, together with our previous study of BC-associated A-BBOA in Tibet, results presented herein demonstrate that A-BBOA could lead to thick coating on BC cores, meaning a significant “lensing effect” to the enhancement of BC light absorption[40]. As a key component of BC coating, presence of this factor may also alter the bulk hygroscopicity of BC-PM_1. It could therefore affect its activation ability as cloud condensation nuclei (CCN)[4]. Overall, the emission, evolution and transport of such A-BBOA, may significantly affect the atmospheric behaviors and influence the role of BC in the air quality and climate (e.g., radiative forcing and precipitation). Future laboratory, field, and modeling studies are required to evaluate the regional environmental impacts of A-BBOA.

ASSOCIATED CONTENT

Supporting Information

AUTHOR INFORMATION

Corresponding Authors

ACKNOWLEDGMENTS

The authors from PRC acknowledge support from the National Natural Science Foundation of China (21777073) and the National Key Research and Development Program of China (No. 2018YFC0213802).The authors from Harvard and NUIST acknowledge additional support through the Harvard-NUIST Joint Laboratory for Air Quality and Climate (JLAQC).

ABBREVIATIONS

BC Black carbon

PM_1 Particulate matter with an aerodynamic diameter smaller than 1 μm

NR-PM_1 non-refractory PM_1

BC-PM_1 BC-containing particles in PM_1

BrC Brown carbon

HR-AMS High-resolution aerosol mass spectrometer (Aerodyne Research Inc.)

SP-AMS Soot-particle aerosol mass spectrometer (Aerodyne Research Inc.)

IE Ionization efficiency

RIE Relative ionization efficiency

HRMS High-resolution mass spectra

PMF Positive matrix factorization

OA Organic aerosol

SOA Secondary organic aerosolO/C Oxygen-to-carbon ratio

H/C Hydrogen-to-carbon ratio

A-BBOA Aged biomass burning organic aerosol

SV-OOA Semi-volatile oxygenated organic aerosol

LV-OOA low-volatility oxygenated organic aerosol

MO-OOA more-oxidized oxygenated organic aerosol

LO-OOA less-oxidized oxygenated organic aerosol

R_{BC} mass ratio of BC coatings to BC

D_{va} Vacuum aerodynamic diameter

REFERENCES

1. Bond, T. C.; Doherty, S. J.; Fahey, D. W.; Forster, P. M.; Berntsen, T.; DeAngelo, B. J.; Flanner, M. G.; Ghan, S.; Kärcher, B.; Koch, D.; Kinne, S.; Kondo, Y.; Quinn, P. K.; Sarofim, M. C.; Schultz, M. G.; Schulz, M.; Venkataraman, C.; Zhang, H.; Zhang, S.; Bellouin, N.; Guttikunda, S. K.; Hopke, P. K.; Jacobson, M. Z.; Kaiser, J. W.; Klimont, Z.; Lohmann, U.; Schwarz, J. P.; Shindell, D.; Storelvmo, T.; Warren, S. G.; Zender, C. S., Bounding the role of black carbon in the climate system: A scientific assessment. *J Geophys Res: Atmos* **2013,** *118*, (11), 5380-5552.

2. Janssen, AH.; Gerlofs-Nijland, E; Lanki, Timo; Salonen, Raimo; Cassee, Flemming; Hoek, Gerard; Fischer, Paul; Brunekreef, Bert; Krzyzanowski, Michal. Health effects of black carbon. **2012**.

3. Ramanathan, V.; Carmichael, G., Global and regional climate changes due to black carbon. *Nature Geosci* **2008,** *1*, (4), 221-227.

4. Wu, Y.; Liu, D.; Wang, J.; Shen, F.; Chen, Y.; Cui, S.; Ge, S.; Wu, Y.; Chen, M.; Ge, X., Characterization of Size-Resolved Hygroscopicity of Black Carbon-Containing Particle in Urban Environment. *Environ Sci Technol* **2019,** *53*, (24), 14212-14221.

5. Lee, A. K. Y.; Chen, C. L.; Liu, J.; Price, D. J.; Betha, R.; Russell, L. M.; Zhang, X.; Cappa, C. D., Formation of secondary organic aerosol coating on black carbon particles near vehicular emissions. *Atmos Chem Phys* **2017,** *17*, (24), 15055-15067.

6. Buseck, P. R.; Adachi, K.; Gelencsér, A.; Tompa, É.; Pósfai, M., Ns-Soot: A Material-Based Term for Strongly Light-Absorbing Carbonaceous Particles. *Aerosol Sci Technol* **2014,** *48*, (7), 777-788.

7. China, S.; Scarnato, B.; Owen, R. C.; Zhang, B.; Ampadu, M. T.; Kumar, S.; Dzepina, K.; Dziobak, M. P.; Fialho, P.; Perlinger, J. A.; Hueber, J.; Helmig, D.; Mazzoleni, L. R.; Mazzoleni, C., Morphology and mixing state of aged soot particles at a remote marine free troposphere site: Implications for optical properties. *Geophys Res Lett* **2015,** *42*, (4), 1243-1250.

8. Saleh, R.; Marks, M.; Heo, J.; Adams, P. J.; Donahue, N. M.; Robinson, A. L., Contribution of brown carbon and lensing to the direct radiative effect of carbonaceous aerosols from biomass and biofuel burning emissions. *J Geophys Res: Atmos* **2015,** *120*, (19), 10,285-10,296.

9. Cappa, C. D.; Onasch, T. B.; Massoli, P.; Worsnop, D. R.; Bates, T. S.; Cross, E. S.; Davidovits, P.; Hakala, J.; Hayden, K. L.; Jobson, B. T.; Kolesar, K. R.; Lack, D. A.; Lerner, B. M.; Li, S.-M.; Mellon, D.; Nuaaman, I.; Olfert, J. S.; Petäjä, T.; Quinn, P. K.; Song, C.; Subramanian, R.; Williams, E. J.; Zaveri, R. A., Radiative absorption enhancements due to the mixing state of atmospheric black carbon. *Science* **2012,** *337*, (6098), 1078-1081.

10. Canagaratna, M. R.; Jayne, J. T.; Jimenez, J. L.; Allan, J. D.; Alfarra, M. R.; Zhang, Q.; Onasch, T. B.; Drewnick, F.; Coe, H.; Middlebrook, A.; Delia, A.; Williams, L. R.; Trimborn, A. M.; Northway, M. J.; DeCarlo, P. F.; Kolb, C. E.; Davidovits, P.; Worsnop, D. R., Chemical and microphysical characterization of ambient aerosols with the aerodyne aerosol mass spectrometer. *Mass Spectrom Rev* **2007,** *26*, (2), 185-222.

11. Li, Y. J.; Lee, B. P.; Su, L.; Fung, J. C. H.; Chan, C. K., Seasonal characteristics of fine particulate matter (PM) based on high-resolution time-of-flight aerosol mass spectrometric (HR-ToF-AMS) measurements at the HKUST Supersite in Hong Kong. *Atmos Chem Phys* **2015,** *15*, (1), 37-53.

12. Lee, B. P.; Li, Y. J.; Yu, J. Z.; Louie, P. K. K.; Chan, C. K., Physical and chemical characterization of ambient aerosol by HR-ToF-AMS at a suburban site in Hong Kong during springtime 2011. *J Geophys Res: Atmos* **2013**, *118* (15) 8625-8639.

13. Sun, Y. L.; Zhang, Q.; Schwab, J. J.; Chen, W. N.; Bae, M. S.; Hung, H. M.; Lin, Y. C.; Ng, N. L.; Jayne, J.; Massoli, P.; Williams, L. R.; Demerjian, K. L., Characterization of near-highway submicron aerosols in New York City with a high-resolution aerosol mass spectrometer. *Atmos Chem Phys* **2012,** *12*, (4), 2215-2227.

14. Ge, X. L.; Setyan, A.; Sun, Y.; Zhang, Q., Primary and secondary organic aerosols in Fresno, California during wintertime: Results from high resolution aerosol mass spectrometry. *J Geophys Res: Atmos* **2012,** *117*, (D19), D19301.

15. Ge, X.; Zhang, Q.; Sun, Y.; Ruehl, C. R.; Setyan, A., Effect of aqueous-phase processing on aerosol chemistry and size distributions in Fresno, California, during wintertime. *Environ Chem* **2012,** *9*, (3), 221-235.

16. Xu, W.; Xie, C.; Karnezi, E.; Zhang, Q.; Wang, J.; Pandis, S. N.; Ge, X.; Zhang, J.; An, J.; Wang, Q., Summertime aerosol volatility measurements in Beijing, China. *Atmos Chem Phys* **2019,** *19*, (15), 10205-10216.

17. Sun, Y.; Jiang, Q.; Wang, Z.; Fu, P.; Li, J.; Yang, T.; Yin, Y., Investigation of the Sources and Evolution Processes of Severe Haze Pollution in Beijing in January 2013. *J Geophys Res: Atmos* **2014**, 2014JD021641.

18. Onasch, T. B.; Trimborn, A.; Fortner, E. C.; Jayne, J. T.; Kok, G. L.; Williams, L. R.; Davidovits, P.; Worsnop, D. R., Soot particle aerosol mass spectrometer: Development, validation, and initial application. *Aerosol Sci Technol* **2012,** *46*, (7), 804-817.

19. Wang, J.; Onasch, T. B.; Ge, X.; Collier, S.; Zhang, Q.; Sun, Y.; Yu, H.; Chen, M.; Prévôt, A. S.; Worsnop, D. R., Observation of fullerene soot in eastern China. *Environ Sci Technol Lett* **2016,** *3*, (4), 121-126.

20. Collier, S.; Zhou, S.; Kuwayama, T.; Forestieri, S.; Brady, J.; Zhang, M.; Kleeman, M.; Cappa, C.; Bertram, T.; Zhang, Q., Organic PM Emissions from Vehicles: Composition, O/C Ratio, and Dependence on PM Concentration. *Aerosol Sci Technol* **2015,** *49*, (2), 86-97.

21. Massoli, P.; Onasch, T. B.; Cappa, C. D.; Nuamaan, I.; Hakala, J.; Hayden, K.; Li, S.-M.; Sueper, D. T.; Bates, T. S.; Quinn, P. K.; Jayne, J. T.; Worsnop, D. R., Characterization of black carbon-containing particles from soot particle aerosol mass spectrometer measurements on the R/V Atlantis during CalNex 2010. *J Geophys Res: Atmos* **2015,** *120*, (6), 2014JD022834.

22. Wang, J.; Zhang, Q.; Chen, M.; Collier, S.; Zhou, S.; Ge, X.; Xu, J.; Shi, J.; Xie, C.; Hu, J., First chemical characterization of refractory black carbon aerosols and associated coatings over the

Tibetan Plateau (4730 m asl). *Environ Sci Technol* **2017,** *51*, (24), 14072-14082.

23. Xu, J.; Zhang, Q.; Shi, J.; Ge, X.; Xie, C.; Wang, J.; Kang, S.; Zhang, R.; Wang, Y., Chemical characteristics of submicron particles at the central Tibetan Plateau: insights from aerosol mass spectrometry. *Atmos Chem Phys* **2018,** *18*, (1).

24. Xie, C.; Xu, W.; Wang, J.; Wang, Q.; Liu, D.; Tang, G.; Chen, P.; Du, W.; Zhao, J.; Zhang, Y., Vertical characterization of aerosol optical properties and brown carbon in winter in urban Beijing, China. *Atmos Chem Phys* **2019,** *19*, (1), 165-179.

25. Liu, D.; Joshi, R.; Wang, J.; Yu, C.; Allan, J. D.; Coe, H.; Flynn, M. J.; Xie, C.; Lee, J.; Squires, F., Contrasting physical properties of black carbon in urban Beijing between winter and summer. *Atmos Chem Phys* **2019,** *19*, (10), 6749-6769.

26. Wang, J.; Liu, D.; Ge, X.; Wu, Y.; Shen, F.; Chen, M.; Zhao, J.; Xie, C.; Wang, Q.; Xu, W., Characterization of black carbon-containing fine particles in Beijing during wintertime. *Atmos Chem Phys* **2019,** *19*, (1), 447-458.

27. Qiu, Y.; Xie, Q.; Wang, J.; Xu, W.; Li, L.; Wang, Q.; Zhao, J.; Chen, Y.; Chen, Y.; Wu, Y., Vertical characterization and source apportionment of water-soluble organic aerosol with high-resolution aerosol mass spectrometry in beijing, china. *ACS Earth Space Chem* **2019,** *3*, (2), 273-284.

28. Xu, W.; Sun, Y.; Wang, Q.; Zhao, J.; Wang, J.; Ge, X.; Xie, C.; Zhou, W.; Du, W.; Li, J., Changes in Aerosol Chemistry From 2014 to 2016 in Winter in Beijing: Insights From High-Resolution Aerosol Mass Spectrometry. *J Geophys Res: Atmos* **2019,** *124*, (2), 1132-1147.

29. Xie, C.; Xu, W.; Wang, J.; Liu, D.; Ge, X.; Zhang, Q.; Wang, Q.; Du, W.; Zhao, J.; Zhou, W., Light absorption enhancement of black carbon in urban Beijing in summer. *Atmos Environ* **2019,** *213*, 499-504.

30. Xu, W.; Xie, C.; Karnezi, E.; Zhang, Q.; Wang, J.; Pandis, S. N.; Ge, X.; Zhang, J.; An, J.; Wang, Q.; Zhao, J.; Du, W.; Qiu, Y.; Zhou, W.; He, Y.; Li, Y.; Li, J.; Fu, P.; Wang, Z.; Worsnop, D. R.; Sun, Y., Summertime aerosol volatility measurements in Beijing, China. *Atmos Chem Phys* **2019,** *19*, (15), 10205-10216.

31. Canagaratna, M. R.; Jimenez, J. L.; Kroll, J. H.; Chen, Q.; Kessler, S. H.; Massoli, P.; Hildebrandt Ruiz, L.; Fortner, E.; Williams, L. R.; Wilson, K. R.; Surratt, J. D.; Donahue, N. M.; Jayne, J. T.; Worsnop, D. R., Elemental ratio measurements of organic compounds using aerosol mass spectrometry: characterization, improved calibration, and implications. *Atmos Chem Phys* **2015,** *15*, (1), 253-272.

32. Paatero, P.; Tapper, U., Positive matrix factorization: A non-negative factor model with optimal utilization of error estimates of data values. *Environmetrics* **1994,** *5*, (2), 111-126.

33. Ulbrich, I. M.; Canagaratna, M. R.; Zhang, Q.; Worsnop, D. R.; Jimenez, J. L., Interpretation of organic components from Positive Matrix Factorization of aerosol mass spectrometric data. *Atmos Chem Phys* **2009,** *9*, (9), 2891-2918.

34. Zhang, Q.; Jimenez, J.; Canagaratna, M.; Ulbrich, I.; Ng, N.; Worsnop, D.; Sun, Y.,

Understanding atmospheric organic aerosols via factor analysis of aerosol mass spectrometry: a review. *Anal Bioanal Chem* **2011,** *401*, (10), 3045-3067.

35. Xu, W.; Sun, Y.; Wang, Q.; Zhao, J.; Wang, J.; Ge, X.; Xie, C.; Zhou, W.; Du, W.; Li, J., Changes in aerosol chemistry from 2014 to 2016 in winter in Beijing: Insights from high-resolution aerosol mass spectrometry. *J Geophys Res: Atmos* **2019,** *124*, (2), 1132-1147.

36. Sun, Y.; Jiang, Q.; Xu, Y.; Ma, Y.; Zhang, Y.; Liu, X.; Li, W.; Wang, F.; Li, J.; Wang, P.; Li, Z., Aerosol characterization over the North China Plain: Haze life cycle and biomass burning impacts in summer. *J Geophys Res: Atmos* **2016,** *121*, (5), 2508-2521.

37. Shen, L.; Jacob, D. J.; Zhu, L.; Zhang, Q.; Zheng, B.; Sulprizio, M. P.; Li, K.; De Smedt, I.; González Abad, G.; Cao, H.; Fu, T.-M.; Liao, H., The 2005–2016 Trends of Formaldehyde Columns Over China Observed by Satellites: Increasing Anthropogenic Emissions of Volatile Organic Compounds and Decreasing Agricultural Fire Emissions. *Geophys Res Lett* **2019,** *46*, (8), 4468-4475.

38. Ng, N. L.; Canagaratna, M. R.; Jimenez, J. L.; Chhabra, P. S.; Seinfeld, J. H.; Worsnop, D. R., Changes in organic aerosol composition with aging inferred from aerosol mass spectra. *Atmos Chem Phys* **2011,** *11*, (13), 6465-6474.

39. Chen, C.; Fan, X.; Shaltout, T.; Qiu, C.; Ma, Y.; Goldman, A.; Khalizov, A. F., An unexpected restructuring of combustion soot aggregates by subnanometer coatings of polycyclic aromatic hydrocarbons. *Geophys Res Lett* **2016,** *43*, (20), 11,080-11,088.

40. Liu, D.; Whitehead, J.; Alfarra, M. R.; Reyes-Villegas, E.; Spracklen, Dominick V.; Reddington, Carly L.; Kong, S.; Williams, Paul I.; Ting, Y.-C.; Haslett, S.; Taylor, Jonathan W.; Flynn, Michael J.; Morgan, William T.; McFiggans, G.; Coe, H.; Allan, James D., Black-carbon absorption enhancement in the atmosphere determined by particle mixing state. *Nature Geosci* **2017,** *10*, (3), 184-188.

List of Figures

TOC

Figure 1. Temporal variations of selected chemical species measured in Beijing on June 4 -29, 2017. (a) mixing ratios of nitrogen dioxide (NO_2) and ozone (O_3); (b) 15-m relative humidity (*RH*) and temperature (*T*); (c-e) on the left are the mass loadings of organic (Org), sulfate (SO_4^{2-}) and nitrate (NO_3^-) measured by HR-AMS and SP-AMS, and on the right are mass ratios of individual BC-PM_1 species to NR-PM_1 species (e.g., BC-PM_1 Org to NR-PM_1 Org). The NR-PM_1 species measured by HR-AMS is in solid line, and the BC-PM_1 species measured by SP-AMS is in the dotted line. The shaded areas are raining periods. The observation period is divided into two cases according to the mixing ratio of nitrogen NO_2, Case I and Case II, which represent high NO_2 and low NO_2 mixing ratios, respectively.

Figure 2. Temporal variations (left panels), high-resolution mass spectra (right panels) of five OA factors in summer 2017: (a) and (f) HOA, (b) and (g) A-BBOA, (c) and (h) OOA1 (LO-OOA), (d) and (i) OOA2, and (e) and (j) OOA3. Also shown in the left panels are the time series of other tracers, including $C_4H_9^+$, NO_x, $C_2H_4O_2^+$, $K_3SO_4^+$, $C_6H_{10}O^+$, $C_2H_3O^+$, SO_4^{2-} and NO_3^-.

Figure 3. Temporal variations of NR-PM_1 and BC-PM_1 (a-c) HOA, LO-OOA, and MO-OOA (left panels) and (d-e) their fractions. NR-PM_1 OA factors are in red, and the BC-PM_1 OA factors are in black. Here BC-PM_1 MO-OOA is the sum of A-BBOA, OOA2 (sulfate-related OOA), and OOA3 (nitrate-related OOA).

Figure 4. Box plots of mass loadings and fractions of five selected species (HOA, LO-OOA, MO-OOA, SO_4^{2-}, and NO_3^-) in Case I and Case II. The bounds of boxes represent quartiles, the whiskers indicate the 90th and 10th percentiles, and the lines and dots inside the boxes are median and mean values. NR-PM_1 OA factors are in red, and the BC-PM_1 OA factors are in black.

Figure 5 Comparison between the high-resolution mass spectra of A-BBOA obtained in Nam Co (June 2015) and Beijing (June 2017).

Figure 6. (a-c) the mass loadings of BC, BC-PM_1 Org, fractions of BC-PM_1 OA factors, E_{abs}, the oxidation state (OSc = 2*(O/C) – (H/C)) of BC-PM_1 Org, and the size distribution of BC-PM_1 Org as a function of coating thickness (R_{BC}). (d) temporal variations of OA fractions of NR-PM_1 and BC-PM_1 from 15:00 to 24:00 on June 17, 2017.

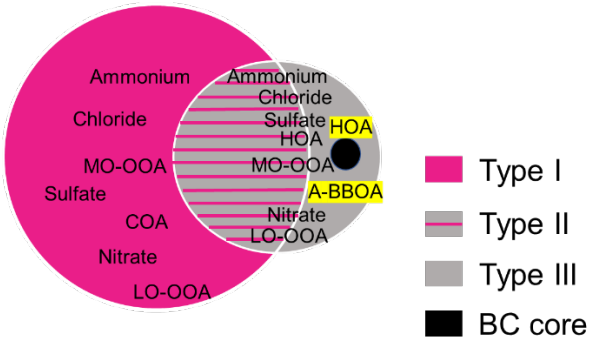
Ammonium
Chloride
MO-OOA
Sulfate
COA
Nitrate
LO-OOA
Ammonium
Chloride
Sulfate
HOA
MO-OOA
A-BBOA
Nitrate
LO-OOA
HOA
Type I
Type II
Type III
BC core

TOC

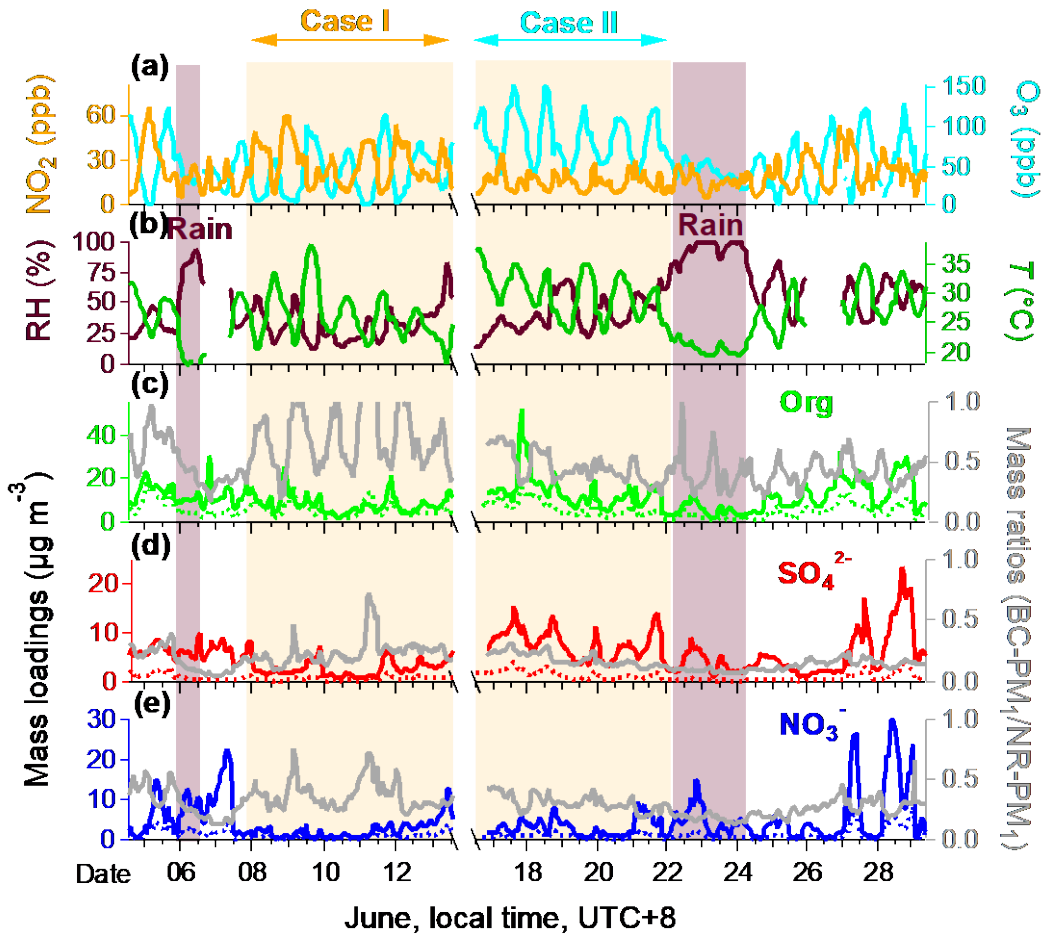

Figure 1. Temporal variations of selected chemical species measured in Beijing on June 4 -29, 2017. (a) mixing ratios of nitrogen dioxide (NO_2) and ozone (O_3); (b) 15-m relative humidity (*RH*) and temperature (*T*); (c-e) on the left are the mass loadings of organic (Org), sulfate (SO_4^{2-}) and nitrate (NO_3^-) measured by HR-AMS and SP-AMS, and on the right are mass ratios of individual BC-PM_1 species to NR-PM_1 species (e.g., BC-PM_1 Org to NR-PM_1 Org). The NR-PM_1 species measured by HR-AMS is in solid line, and the BC-PM_1 species measured by SP-AMS is in the dotted line. The shaded areas are raining periods. The observation period is divided into two cases according to the mixing ratio of nitrogen NO_2, Case I and Case II, which represent high NO_2 and low NO_2 mixing ratios, respectively.

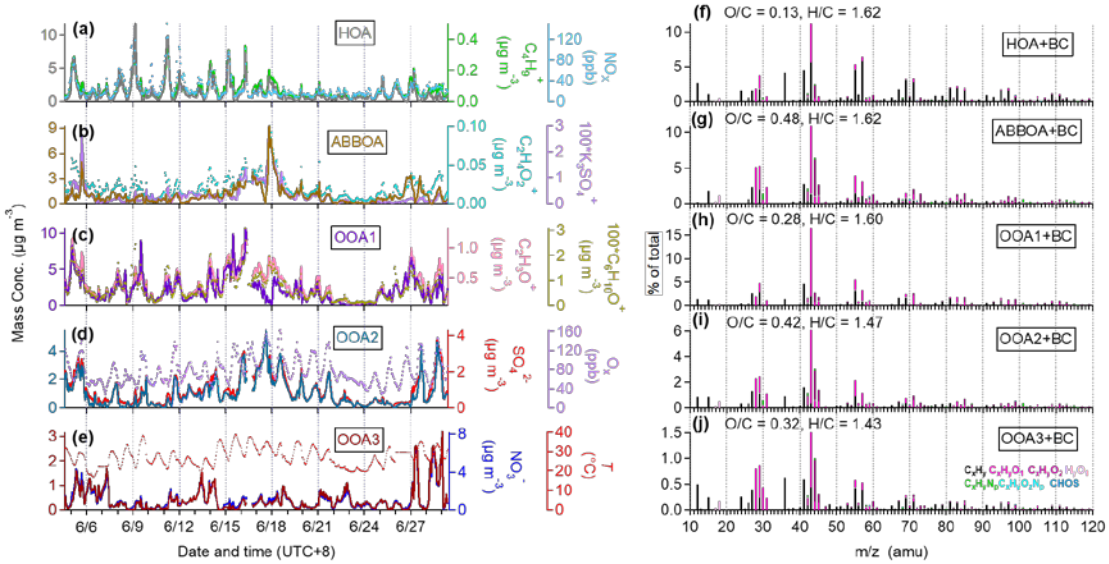

Figure 2. Temporal variations (left panels), high-resolution mass spectra (right panels) of five OA factors in summer 2017: (a) and (f) HOA, (b) and (g) A-BBOA, (c) and (h) OOA1 (LO-OOA), (d) and (i) OOA2, and (e) and (j) OOA3. Also shown in the left panels are the time series of other tracers, including $C_4H_9^+$, NOx, $C_2H_4O_2^+$, $K_3SO_4^+$, $C_6H_{10}O^+$, $C_2H_3O^+$, SO_4^{2-} and NO_3^-.

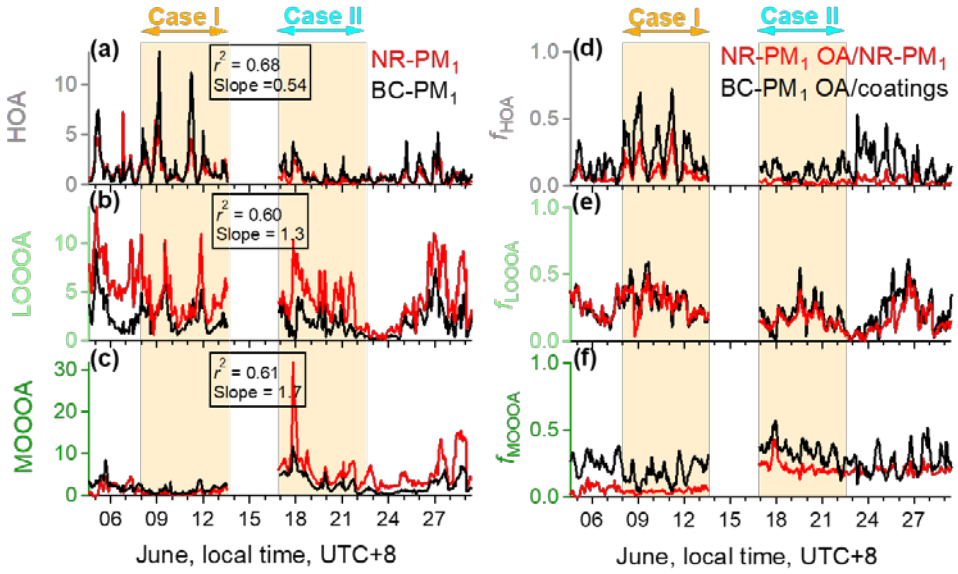

Figure 3. Temporal variations of NR-PM_1 and BC-PM_1 (a-c) HOA, LO-OOA, and MO-OOA (left panels) and (d-e) their fractions. NR-PM_1 OA factors are in red, and the BC-PM_1 OA factors are in black. Here BC-PM_1 MO-OOA is the sum of A-BBOA, OOA2 (sulfate-related OOA), and OOA3 (nitrate-related OOA).

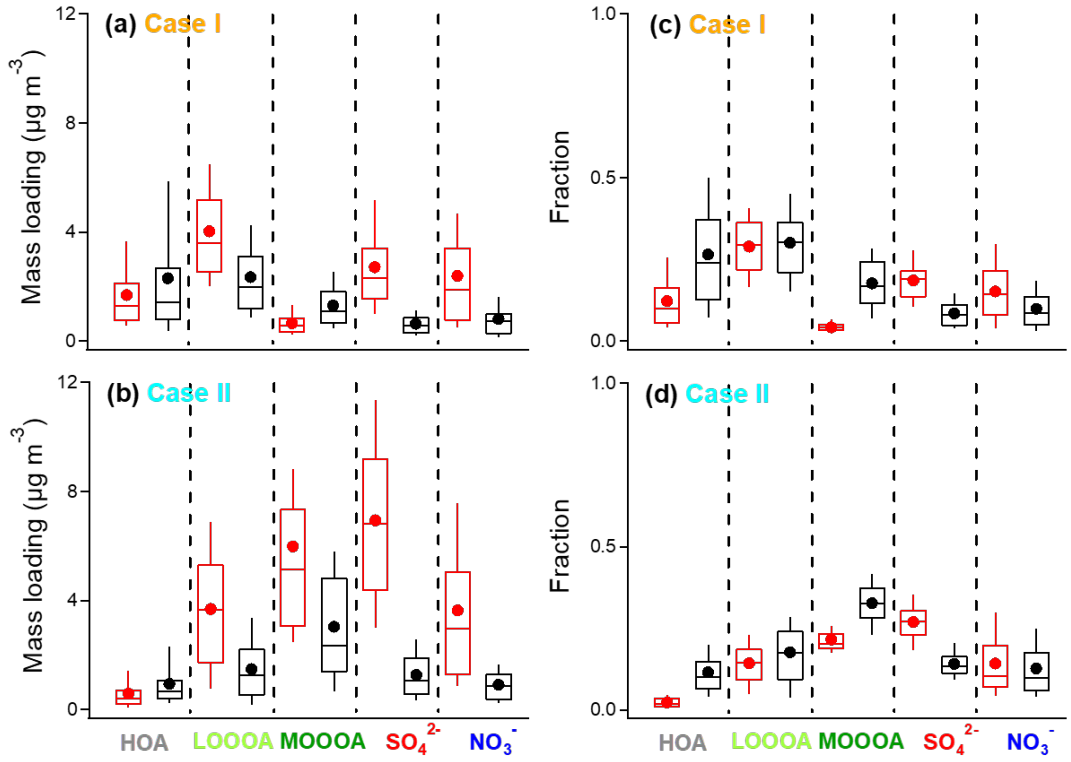

Figure 4. Box plots of mass loadings and fractions of five selected species (HOA, LO-OOA, MO-OOA, SO_4^{2-}, and NO_3^-) in Case I and Case II. The bounds of boxes represent quartiles, the whiskers indicate the 90th and 10th percentiles, and the lines and dots inside the boxes are median and mean values. NR-PM_1 OA factors are in red, and the BC-PM_1 OA factors are in black.

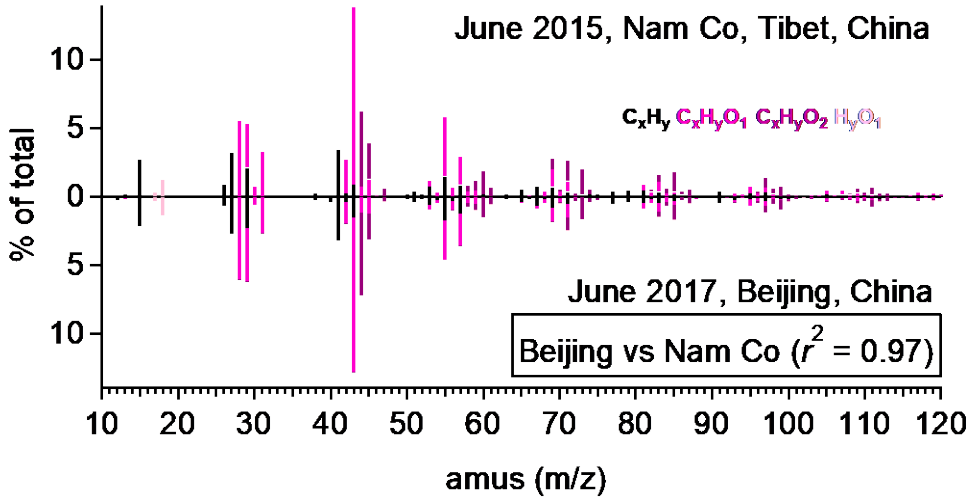

Figure 5 Comparison between the high-resolution mass spectra of A-BBOA obtained in Nam Co (June 2015) and Beijing (June 2017).

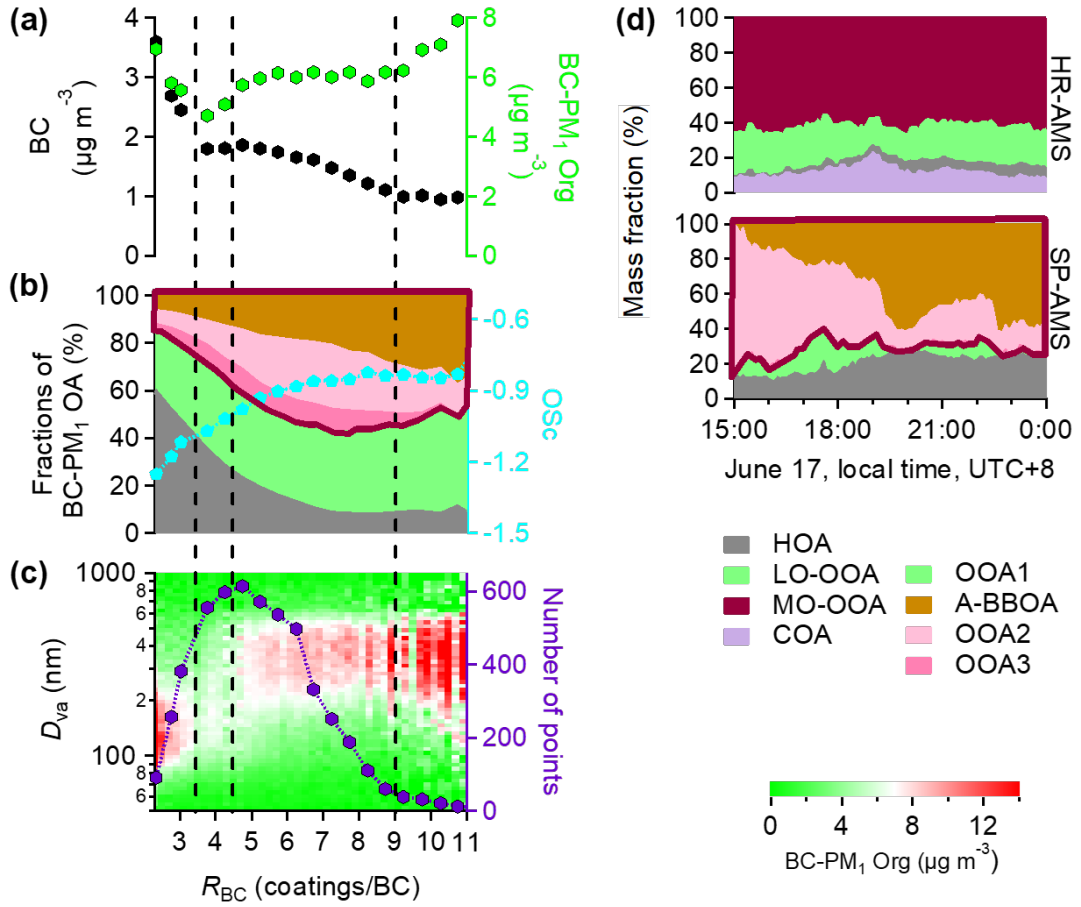

Figure 6. (a-c) the mass loadings of BC, BC-PM_1 Org, fractions of BC-PM_1 OA factors, E_{abs}, the oxidation state (OSc = 2*(O/C) – (H/C)) of BC-PM_1 Org, and the size distribution of BC-PM_1 Org as a function of coating thickness (R_{BC}). (d) temporal variations of OA fractions of NR-PM_1 and BC-PM_1 from 15:00 to 24:00 on June 17, 2017.